Fundamental investigation of dry electrical discharge machining (DEDM) by optical emission spectroscopy and its numerical interpretation

Author(s):
Macedo, Felipe T.B.; Wiessner, Moritz; Hollenstein, Christoph; Esteves, Paulo M.B.; Wegener, Konrad

Publication date:
2017-06

Permanent link:
https://doi.org/10.3929/ethz-b-000122449

Originally published in:
The International Journal of Advanced Manufacturing Technology 90(9-12), https://doi.org/10.1007/s00170-016-9687-9

Int J Adv Manuf Technol (2017) 90:3697–3709
DOI 10.1007/s00170-016-9687-9

ORIGINAL ARTICLE

Fundamental investigation of dry electrical discharge machining (DEDM) by optical emission spectroscopy and its numerical interpretation

Felipe T. B. Macedo[1] · **Moritz Wiessner**[1] · **Christoph Hollenstein** · **Paulo M. B. Esteves**[1] · **Konrad Wegener**[1]

Received: 23 July 2016 / Accepted: 31 October 2016 / Published online: 12 November 2016

Abstract Dry electrical discharge machining (DEDM) has been developed as an alternative manufacturing process to the traditional EDM in liquid dielectric media. The absence of the liquid dielectric allows DEDM to be performed by simpler and environmentally friendlier machines. The erosion in DEDM mainly occurs due to the bombardment of the workpiece electrode surface by charged particles produced by micro electric discharges. Thus, the understanding of the fundamental properties of the micro plasma is necessary to explain the erosion mechanisms in this process. Optical emission spectroscopy of DEDM single discharges and its numerical interpretation by emission spectra simulation are developed in the present work. The hypothesis of plasmas in local thermal equilibrium (LTE) is developed, whereas the formation of an electron beam in non-LTE plasmas is also considered and briefly introduced. The simulations show that large amount of different ionic species is produced from the anode workpiece material, and the estimated electron temperature profile is peaking at the plasma centre. Moreover, hot anode spots formed on the workpiece surface due to the plasma-material interactions seem to be considerably smaller than the total plasma diameter and the respective eroded crater. These characteristics indicate that DEDM produces discharges similar to anode dominated vacuum arcs, which present properties very different from EDM discharges in liquid dielectric.

✉ Felipe T. B. Macedo
felipeb@ethz.ch

[1] Institute of machine tools and manufacturing (IWF), ETH Zurich, Zurich, Switzerland

Keywords Dry electrical discharge machining (DEDM) · Emission spectra simulation · Optical emission spectroscopy · Plasma in micro gaps

1 Introduction

Electrical discharge machining (EDM) is a widely applied non-conventional manufacturing process. In EDM, material removal from the workpiece occurs due to its interactions with electric discharge plasmas formed in a liquid dielectric medium, which isolates tool and workpiece electrodes. Deionized water or hydrocarbon oil are commonly used as dielectric media, depending on the application. Oil-based dielectric media, mostly applied in die-sinking EDM, generate toxic gases and non-environmentally friendly waste during the erosion process, as infer Leão et al. [1].

Dry electrical discharge machining (DEDM) has been presented as an alternative to the conventional EDM process. DEDM works with gases instead of liquid dielectric media. Simpler and environmentally friendlier machines can perform the machining process due to the absence of liquid dielectric. Usually, high-pressure gas is flushed through a thin-walled pipe tool electrode in DEDM. The gas flow enlarges the material removal rate (MRR) due to the flushing of eroded particles out of the inter-electrode gap, as proposed by Kunieda et al. [2]. Several authors [3–12, 2] have reported that DEDM can provide larger MRR, lower surface roughness and smaller heat-affected zones on the workpiece surface. Moreover, the tool electrode wear can be very small and independent of the discharge pulse duration, differently than EDM in liquid dielectric media.

The research efforts in DEDM have increased during the last years due to the referred advantages and process strengths. In 1985, the National Aeronautics and Space Administration

(NASA) reported DEDM for the first time [13], applying argon and helium as dielectric media. Later, Kunieda et al. [2] presented benefits of DEDM in air as dielectric. Since then, different technologies have been developed in order to improve DEDM, in particular hybrid processes. Kunieda et al. [11] applied piezoelectric actuators to provide a better frequency response of the gap control in DEDM. According to their results, the stabilization of the inter-electrode gap by the piezoelectric servo system was able to provide larger MRR. Zhang et al. [14] presented enhancements in MRR by applying ultrasonic-assisted DEDM process. Joshi et al. [15] developed a DEDM process assisted by pulsating magnetic fields, which provide increase in MRR and improvements in eroded surface quality. Shen et al. [16] showed that a combination of large energy levels, long discharge pulses, strong gaseous dielectric flushing and high tool electrode rotation significantly increases MRR in DEDM. Furthermore, Tao [17] has published several results showing that gas-liquid mixtures can lead to higher MRR and better surface qualities. Despite the efforts made in order to optimize DEDM performance, several phenomena involved in this process are still not well explained. Proper understanding of the fundamentals of DEDM is necessary to allow future development of this manufacturing technology.

As in conventional EDM, erosion of the workpiece in DEDM occurs due to the bombardment of its surface by charged particles produced by micro electric discharges. Nevertheless, the properties of the DEDM plasma and its interactions with electrode material are considerably different from EDM in liquid. Kanmani Subbu et al. [18] presented the first systematic investigation regarding DEDM plasmas using optical emission spectroscopy. The results show that DEDM plasmas are considerably less dense than the ones obtained by EDM in liquids. Recently, Macedo et al. [19] presented time-dependent electron temperature (T_e) and electron density (N_e) average measurements in DEDM from optical emission spectroscopy. The electron temperatures were calculated from the two-line Boltzmann method, and the density was obtained from H_α Stark broadening. Nonetheless, detailed information concerning electron density, electron temperature and particle composition of the DEDM plasmas is still lacking.

Optical emission spectroscopy and high-speed imaging are some of the rare plasma diagnostic techniques that can be properly used for direct characterization of DEDM micro plasmas. Properties of the plasma can also be indirectly deduced by electrical parameter measurements and crater observations. Correlation between data obtained from those different measurement methods, direct and indirect, can help to understand the phenomena involved in DEDM.

Together with modern optical equipment, existing commercial software can help to provide new advanced interpretation of optical emission spectra, giving new insight into the plasma physics. Thanks to the advance in collecting basic data and information on atomic and molecular physics, various models can be applied to calculate optical spectra. This calculation is currently possible for almost all atoms and molecules under nearly all plasma conditions.

In the present paper, the strength of software application to support interpretation of optical emission spectra of metallic DC plasmas is presented. Applying the commercially available PrismSPECT [20], the measured optical emission spectra are simulated using a collisional-radiative (CR) model to obtain as much information on the plasma as possible. Line intensities, intensity ratios, line broadening and spectra fitting allow obtaining detailed information on plasma components, such as particle and excitation population densities, electron density and electron temperature. It allows obtaining indications on the plasma parameter profiles, which are deduced by spectra fitting.

Descoeudres [21] infers that plasmas produced by EDM in liquid dielectric media are in local thermal equilibrium (LTE). It is not yet known if this phenomenon also occurs in DEDM. A geometrical constriction of the DEDM plasma could lead to a non-Maxwellian electron energy distribution, such as an electron beam. Under this condition, the plasma is not in LTE, leading to a completely different interpretation of the emission spectra. The LTE plasma hypothesis is developed in this work, whereas the possibility of an electron beam formed in the DEDM plasmas is just briefly presented as a potential further development.

The spectroscopy results are associated with the acquired high-speed imaging, electrical parameters and craters left by single DEDM discharges. It helps to obtain a clearer picture of the DC discharges in the micro gap. The plasma temperature profiles and their resulting spatial distribution of atomic and ionic species can provide indications regarding the important energy distribution on the workpiece surface, crucial for efficient machining.

It is important to emphasize that the research here developed concerns the analysis of single electric discharges, whereas the material removal in the DEDM process occurs by several subsequent discharges. Different pause durations between electric discharges may lead to different plasma properties in DEDM, such as already reported by Maradia [22] for EDM in hydrocarbon oil. Thus, effects of multiple electric discharges and their resulting micro plasmas are not considered in the scope of the present work and need further investigation.

2 Principles

The understanding of the DEDM breakdown mechanisms and discharge properties are necessary in order to characterize the DEDM plasmas. The electrical breakdown of gas discharges

is explained by the avalanche model and the streamer theory, proposed by Loeb and Meek [23] in 1941. According to this theory, a streamer originates the gas discharge. It consists in a weakly ionized channel, rapidly formed in the inter-electrode gap from an intensive primary electron avalanche starting from the cathode. More details about this are described by Raizer [24].

The electrical breakdown voltage of gas discharges can be estimated from the well-known Paschen's law. The Paschen's law calculates the breakdown voltage as a function of the product between the inter-electrode gap size and the gas pressure. The breakdown voltage decreases when the referred product becomes smaller; however, below a critical value of the product, the breakdown voltage increases again. This rise in breakdown voltage takes place due to the electron mean free path, which gets larger than the gap size. Higher voltage is therefore required in order to ensure ionization to start electron avalanches, as explained by Meek and Craggs [25].

Deviations from Paschen's law have been reported for inter-electrode gaps smaller than 5 μm. Breakdown voltages below the Paschen's curve have been registered, independently of the gas pressure. It occurs if at least one of the electrodes, anode or cathode, is made of metallic material. A different kind of electric discharge is formed under this particular condition. This phenomenon has been reported in the literature for different gases [26–30]. The reason for deviations from Paschen's law is a different electrical breakdown mechanism. The electric discharges are produced due to high electric fields generated in the small gap, as explained by Klas et al. [30]. The mechanism is similar to the vacuum breakdown and consists in formation of ion-enhanced field emissions. The referred deviations of the breakdown voltage from Paschen's law for different metallic electrode materials are presented in Fig. 1.

According to Roth et al. [10], DEDM plasmas are generated from a mechanism similar to a vacuum breakdown under the commonly applied electrical parameters. Optical emission spectroscopy of DEDM plasmas earlier published [19] leads to the supposition that hot anode vacuum arcs (HAVA) are formed. HAVA play an important role in several vacuum arc deposition applications and are well described in the literature [31, 32].

A HAVA occurs if sufficient material from the anode is involved to sustain the vacuum arc. The discharge normally starts as a diffuse vacuum arc, burning in material originating from the cathode. However, a cathode with point-type geometry can lead to the concentration of the discharge to a hot anode spot, which becomes an intensive source of metal vapour. The hot anode spot is a region with high temperature and concentration of electrons near the anode surface, as described by Jakubowski et al. [33]. Relatively little cathode activity occurs, and the temperature of the anode is high enough to provide the metal vapour in which the arc burns. The cathode mainly works as a source of electrons, and its potential drop is much less than in other vacuum arcs, whereas the anode and the plasma in the inter-electrode gap provide most of the energy to the discharge, as explained by Boxman et al. [31].

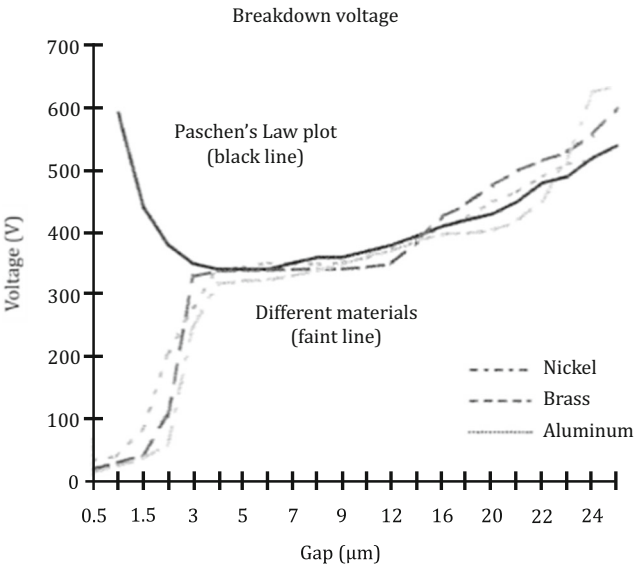

Fig. 1 Breakdown voltages in air versus gap at atmospheric pressure for different metallic electrode materials [27]

There are regions of the plasma in the HAVA discharge where relatively high particle accelerations can occur, which can lead to considerable anode material erosion. High electron energy and a positive plasma potential near the anode were reported in HAVA due to constrictions of the discharge to the anode spot. Bacon et al. [34] show that the constriction causes higher current density near the anode than in the unconstricted plasma column, creating a region of intense evaporation followed by ionization.

The small electric discharge area provided by the thin-walled pipe tool electrodes, commonly applied in DEDM, can concentrate the discharge to a hot anode spot. The generation of hot anode dominated vacuum arcs is probably the main reason for relatively large workpiece material removal and very little tool electrode wear in this process, independently of the discharge pulse duration. Furthermore, the cathode tool electrode is normally coated by material from the anode, which provides negative net cathode erosion, phenomenon also reported in DEDM by ZhanBo et al. [3].

3 Experimental setup

The experimental setup for electric discharge generation consists of a Form 1000 EDM Agie machine. The machine is adapted to perform single electric discharges by a transistor-type generator, which controls the electric current. The single electric discharges are produced applying open voltage of U_{open} = 250 V, discharge current of I = 20 A and pulse duration of t = 316 μs. Moreover, the discharges are performed

moving the tool electrode towards the workpiece with the open voltage. The servomotor of the EDM machine automatically stops when the electrical breakdown occurs.

A Leica DCM 3D confocal microscope is used to measure the 3D profiles of the craters left by the single discharges. Electrical data from the discharges are acquired and measured by a LeCroy Wave Runner 44MXi-A oscilloscope connected to voltage and DC current probes.

The electric discharges are drawn in a point-to-plane electrode configuration. The cathode (tool) is a cylindrical copper electrode of 1 mm diameter with a conical extremity. The anode (workpiece) is a flat surface aluminium electrode. Only this configuration of electrode polarity is discussed in the present paper. The reverse polarity leads to different plasma emission spectra and still needs additional investigation.

High purity levels of the materials are used in the experiments to facilitate the interpretation of the emission spectroscopy achieved data. Aluminium is applied as workpiece material, although it is not commonly machined by EDM. The selection of aluminium for the present investigation is particularly due to its well-known plasma emission spectra, allowing interpretation of the experimental data. Air at atmospheric pressure is used as dielectric medium.

Light emission spectroscopy is performed using an Acton Research Spectrograph 0.275 m connected to a Vision Research Phantom V12.1 high-speed camera (one million frames/s and 300 ns exposure time). The light emitted by the micro electric discharge plasma is guided into the spectrograph by an optical fibre bundle, which has its input positioned near the erosion gap. Emission spectra recorded from different regions within the plasma are integrated by summing the light acquired by all the optical fibres. The used high-speed camera also allows recording the expansion of the plasma plume. Fig. 2 presents a schematic drawing of the optical emission spectroscopy experimental setup, whereas time-resolved emission spectra of a single DEDM discharge are shown in Fig. 3.

4 High-speed imaging

The size of the DEDM plasma channel is linked to the observed light plume around the electrodes emitted during the discharge. The plasma plume dimension is an important input for the interpretation of the emission spectra, as will be shown later. High-speed imaging experiments are performed to measure the plasma plume expansion as function of time. As reported by Macedo et al. [35], the acquisition of black body radiation by the high-speed imaging can lead to difficulties in the DEDM plasma thickness measurements. In order to avoid this, optical filters can be used to record just the light emitted by the plasma. The electrical parameters and electrode materials here applied did not lead to large debris removal by the

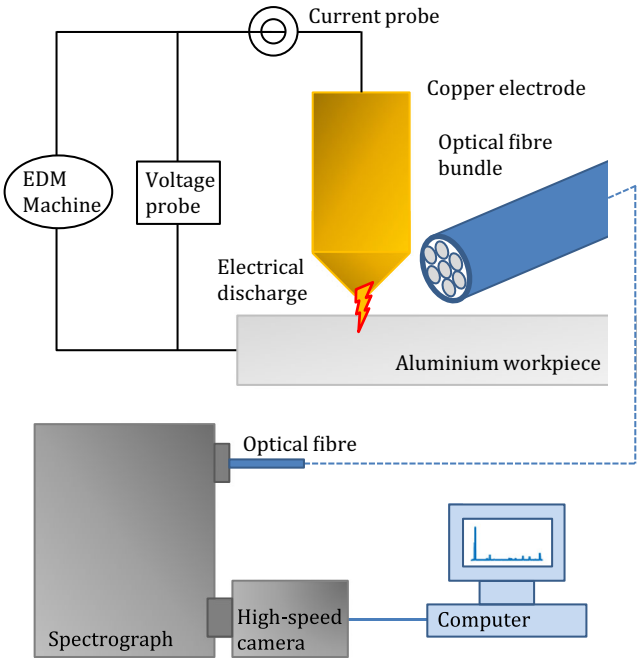

Fig. 2 Experimental setup for plasma emission spectroscopy

discharges. Therefore, no optical filters are used, and the plasma plume expansion is measured directly from the high-speed camera output. Fig. 4 shows a typical image from the high-speed camera, as used for the measurements of plasma plume expansion.

High-pressure gas flow into the erosion gap, commonly used in DEDM, could possibly increase removal of the molten workpiece material during the process and even affect the plasma plume here studied. However, these phenomena are not observed due to the adopted experimental setup, which uses air at atmospheric pressure as dielectric. The small

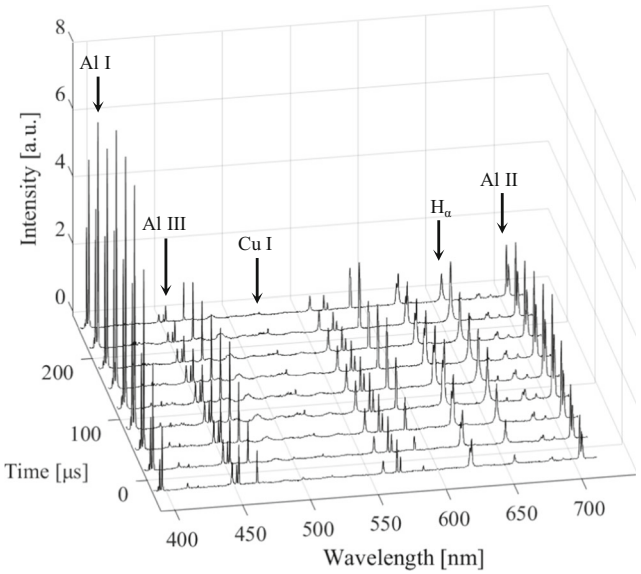

Fig. 3 Time-resolved emission spectra of a single electric discharge [19]; U_{open} = 250 V; I = 20 A; t = 316 μs; Cu cathode; Al anode

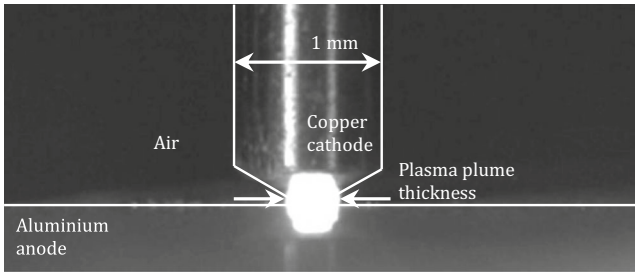

Fig. 4 High-speed imaging experiment; U_{open} = 250 V; I = 20 A; t = 316 μs; Cu cathode; Al anode

amount of particles expelled during the plasma-material interactions suggests that most of the molten material stays in the crater region. The material removal probably takes place due to its evaporation during the discharge.

The plasma rapidly expands at the beginning of the discharge, reaching nearly 200 μm in less than 10 μs, as shown in Fig. 5. Kojima et al. [36] reported also fast plasma plume expansions in air in just a few microseconds for DEDM discharges. The plasma plume size increases just slightly afterwards, and its dimension, around 400 μm, becomes quite stable after 180 μs.

The current is interrupted at the 316 μs of the discharge; even so, visible light is still detected later in time. This emitted light is originated from the afterglow of the discharge, once the power source is stopped.

The craters left by DEDM single discharges on the workpiece surface are measured by confocal microscopy. The average crater diameter is about 185 μm. This value is considerably lower than the total measured plasma dimension (~400 μm). Plasma sizes of DEDM discharges much larger than the respectively left crater were already reported by Kojima et al. [36]. It might mean that DEDM plasmas are spatially inhomogeneous, presenting different properties over their cross section. Moving radially from the central axis (z) of the plasma column, there is a decrease in temperature, and with this, a reduction in electric current. It probably occurs due to the concentration of the discharge to an anode hot spot.

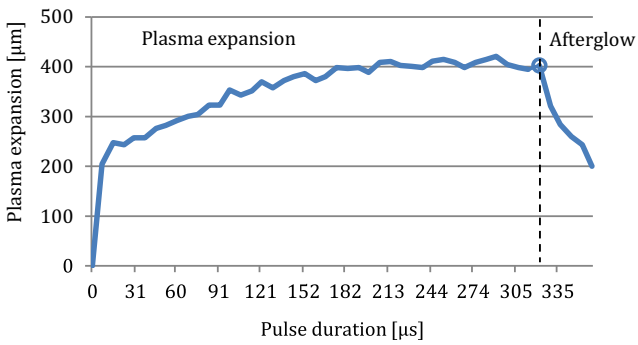

Fig. 5 Plasma plume expansion; U_{open} = 250 V; I = 20 A; t = 316 μs; Cu cathode; Al anode

Thus, regions of the plasma of higher temperature can lead to stronger erosion effects. A schematic temperature profile of the plasma column is shown in Fig. 6.

5 Simulations of optical emission spectra

In order to characterize the DEDM discharge plasma in detail, the measured emission spectra are interpreted using numerical simulations. The method relies on a direct comparison between experimental and simulated spectra using one of the several existing commercial software tools for low-temperature emission spectra calculations. In the following, details on the simulation, comparison and interpretation of the optical emission spectra of the micro discharges in DEDM are presented.

5.1 Collisional-radiative models

Plasmas emit and absorb electromagnetic radiation, such as Bremsstrahlung, recombination and line radiation. Kunze [37] explains that a specific spectral line is emitted by an atom or an ion in a plasma when a bound electron undergoes a transition from an upper (p) to a lower level (q) of energy. The density $n_z(p)$ of the species of charge (z) in the upper state is simply proportional to the transition of the upper to the lower levels expressed by the following:

$$-\left.\frac{dn_z(p)}{dt}\right|_{p\to q} = A(p\to q)n_z(p), \tag{1}$$

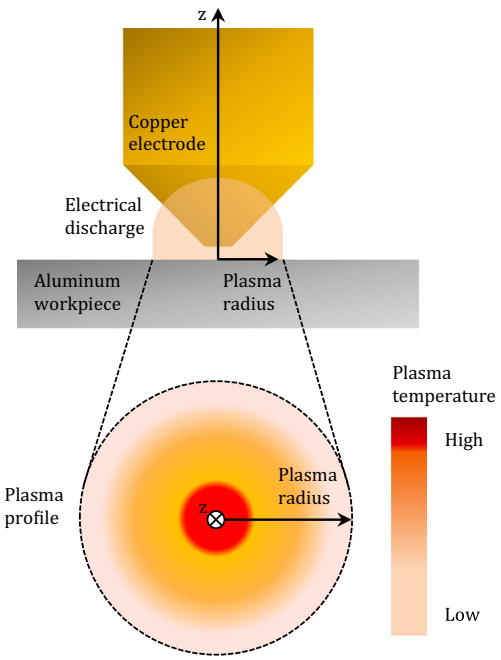

Fig. 6 Schematic plasma temperature profile

where $A(p \rightarrow q)$ is a characteristic atomic constant for that specific transition, and it is known as atomic transition probability or Einstein coefficient of spontaneous emission (s^{-1}). A photon is emitted with each transition, and the emission coefficient ε of the line is thus given by the following:

$$\varepsilon(p \rightarrow q) = \frac{h\nu_{pq}}{4\pi} A(p \rightarrow q) n_z(p), \quad (2)$$

where ν_{pq} is the frequency of the emitted line and h is the Planck constant. This fundamental spectroscopic equation shows that the population densities $n_z(p)$ of the excited states of the atomic species are quantities that can be obtained from measurements of the radiance of lines. The kinetics of the local population of atomic states (p) of ions of charge (z) in plasmas is governed by coupled rate equations of the type

$$\frac{dn_z(p)}{dt} = -R_z(p \rightarrow) + R_z(\rightarrow p) + \Gamma_z(p), \quad (3)$$

where $R_z(p \rightarrow)$ and $R_z(\rightarrow p)$ consist, respectively, in the sums of all rates of possible radiative and collisional transitions out of the level (p) and into the level, whereas $\boldsymbol{\Gamma}_z(p)$ is the external flux of level p population by diffusion and convection. According to Kunze [37], a general solution for this equation is practically impossible due to the large number of transitions that have to be considered and by the fact that, for many transitions, the probabilities and rate coefficients are not properly know.

The CR models have been presented as an approach to reduce the referred coupled rate equations to a set of tractable size by taking into account only the most relevant processes and by considering the pertinent time scales. Kunze [37] proposes a CR model that considers all excited levels in quasi-equilibrium with their ground state and processes, such as electron collisional transitions, radiative decay, collisional ionization, radiative and dielectronic recombination. It leads to a set of coupled linear equations, solved for assumed input ground-state densities $n_z(g)$ and $n_{z+1}(g)$, of the type

$$\frac{dn_z(g)}{dt} = -n_e n_z(g) S_z^{\text{eff}}(T_e, n_e) + n_e n_{z+1}(g) \alpha_{z+1}^{\text{eff}}(T_e, n_e), \quad (4)$$

where S_z^{eff} and $\alpha_{z+1}^{\text{eff}}$ are, respectively, the collisional-radiative ionization and recombination coefficients. These coefficients are both functions of electron temperature and density of the plasma.

CR models can be used to produce synthetic spectra due to the known relation between the radiance of the studied spectral lines with electron temperature (T_e) and density (N_e) of the plasma. The generated synthetic spectra, which are also calculated based on the plasma size, can be compared to the ones obtained by optical emission spectroscopy in order to deduce important plasma parameters.

The commercial PrismSPECT code [20] is used in the present work to calculate the emission spectra of DEDM metal DC plasmas. The CR models used in PrismSPECT are part of the physics package contained in SPECT3D imaging and spectral analysis suit, which calculates the emission spectra of steady state or transient-state plasmas. According to MacFarlane et al. [20], this package is applied in post-processing output from radiation-hydrodynamics codes and particle-in-cell (PIC) codes.

PrismSPECT considers several plasma and atomic physics phenomena and reactions, such as electron-impact ionization, recombination, excitation, deexcitation, radiative recombination, spontaneous decay, dielectronic recombination, autoionization, electron capture, photoionization and photoexcitation. The line and continuum intensities are calculated from transition probabilities of the materials used as tool and workpiece. Furthermore, PrismSPECT takes into account all relevant line-broadening mechanisms, such as Doppler, natural and Stark broadening.

PrismSPECT simulates emission spectra of plasmas in LTE or non-LTE conditions. Effects of non-Maxwellian electron energy distributions onto the emission spectra can be calculated. Moreover, spectra of plasma containing a mixture of different atoms can also be simulated. This is particularly important if different anode and cathode electrode materials are used in DEDM, as in the present case.

Fundamental input plasma parameters applied to calculate the synthetic emission spectra are the plasma temperature, density of charged particles, plasma dimension, plasma geometry and fraction of the different species originating from electrode materials and gaseous dielectric medium. The software allows direct comparison of the simulated spectra with experimental measurements, such as time-resolved and time-integrated spectra, space-resolved spectra and streaked spectra, as described in detail by MacFarlane et al. [20].

5.2 Synthetic spectra calculations

The density of charged particles in the plasma is determined from the line broadening of the H_α line. This is possible since hydrogen is present in the discharge in all investigated cases. The broadening of the H_α line is dominated by the Stark effect, which is associated with the electron density in the plasma, according to Gigosos et al. [38]. The electron density of the plasma is assumed to have a constant spatial profile for the following described fitting procedures. The density is estimated by matching the experimental and simulated H_α emission line either by using line fitting with PrismSPECT or applying theories such as described by Griem [37].

As second input, the plasma temperature of the investigated discharges is needed. DEDM micro plasmas have low electron temperatures, according to results earlier reported [19] for the same experimental setup as considered here. These

electron temperatures are estimated from calculations based on relative intensities of different emission lines of the experimental spectra, as proposed by Griem [39]. Therefore, the emission spectra simulation is performed using the low-temperature plasma data of PrismSPECT.

The hypothesis of Maxwellian electron energy distribution of the electric discharge plasmas is considered and developed in the present approach, as previously mentioned. Additionally, in a first step for simplification, plane geometry of the plasma is defined for the simulations.

The steady-state rate equations of the CR model are solved for the different time steps during the discharge. As composition of the plasma, materials of the electrodes (copper and aluminium) and hydrogen are set in the simulations. The measured emission spectra contain mainly aluminium spectral lines, originating from different Al ionic states, as shown in Fig. 7. Only small intensities of some neutral copper lines have been detected with the applied electrode polarity. In addition, some molecular lines from nitrogen can be found. The peak at the wavelength 589 nm is attributed to the emission lines from a N_2 band, originated from nitrogen of the surrounding atmosphere. The light of this N_2 band might be emitted from the outer part of the plasma plume, and it has not been modelled. Since vacuum discharges are dominated by metallic species, the presence of N_2 probably does not affect the characteristics of the plasma and its interactions with the electrodes material significantly.

The emission spectra simulations show by varying the plasma size at constant electron temperature and electron density that the main emission lines of the studied plasmas are optically thin. It means that self-absorption of the plasma light can be neglected. It has also to be mentioned that some emission lines become optically thick for plasma dimensions varying between 0.5 and 1 mm. Fig. 7 presents a fit between experimental and synthetic spectra. The simulated spectrum is calculated for an electron temperature T = 15,000 K.

The experimental and calculated Al I and Al II emission lines are found to properly match at T = 15,000 K. Nevertheless, no noticeable Al III emission lines are found for this electron temperature condition, as highlighted in the inlet of Fig. 7. Al I lines are emitted by the neutral excited Al population, whereas Al II and Al III are lines emitted by the excited Al^{+1} and Al^{+2} ion populations of the plasma.

Fig. 8 presents a comparison between the same experimental spectrum shown in Fig. 7 and a synthetic spectrum calculated for a higher electron temperature, T = 20,800 K. On the one hand, at higher electron temperature, but the same plasma size and electron density, matching between the most prominent Al II and Al III experimental and calculated emission lines is obtained. On the other hand, Al I lines, as shown in the inset of Fig. 8, have much lower intensity or are even not present in the synthetic spectrum. Therefore, a calculation with a single electron temperature does not allow fully explaining the experimental spectra observed in the DEDM plasma. This result clearly evidences that the DEDM plasma must have a particular temperature profile, as previously suggested by Kojima et al. [36].

An important consideration is the fact that the plasma spectroscopy here performed is not spatially resolved. It means that light from the whole plasma is integrated to generate single spectra. Therefore, it is assumed that some spectral lines, which are excited under a certain electron temperature, are probably emitted from specific plasma regions.

Assuming plane geometry and negligible reabsorption of radiation within the plasma, the light intensity detected by the optical fibre is proportional to the radiance L defined by the following:

$$L = \int \varepsilon(s)\, ds, \tag{5}$$

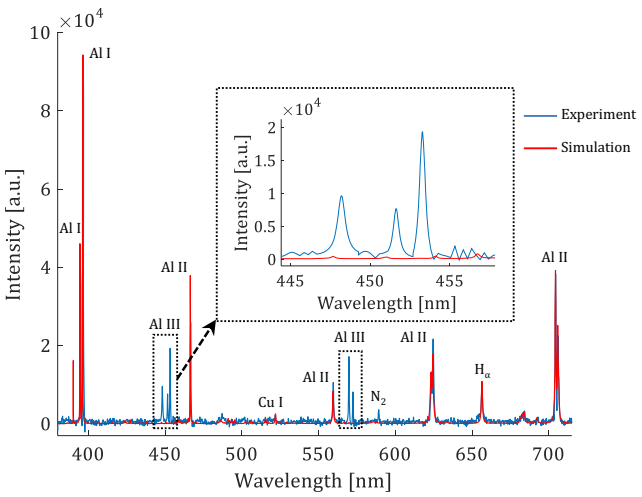

Fig. 7 Experimental and simulated emission spectra; simulated electron temperature T = 15,000 K

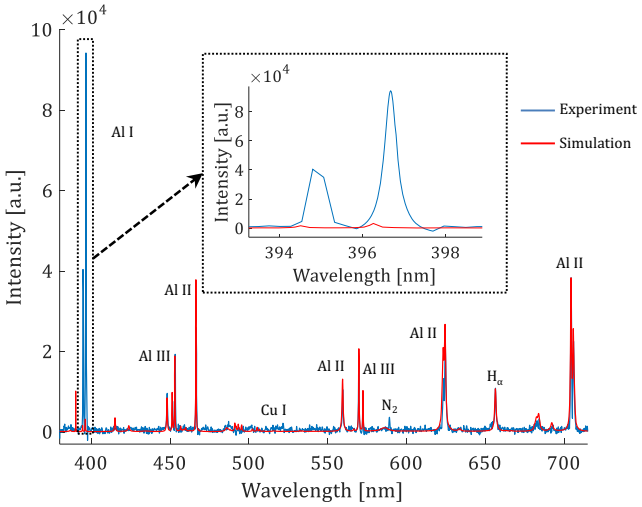

Fig. 8 Experimental and simulated emission spectra; simulated electron temperature T = 20,800 K

where s is line of sight within the plasma and ε is the emission coefficient. $\varepsilon(s)$ depends on plasma parameters, such as electron temperature, electron density and plasma composition. The line of integration is performed over the entire line of sight within the plasma. For a piecewise constant $\varepsilon(s)$, this line integral can be approximated by the following:

$$L \approx \sum_{i}^{N} \varepsilon(s_i)\ \Delta s_i, \tag{6}$$

where $\varepsilon(s_i)$ is the constant emission coefficient in the interval Δs_i and N is the number of zones within the plasma with constant emission coefficient. $\varepsilon(s)\Delta s_i$ can be obtained from the CR model such as described by Kunze [37] or calculated directly by the PrismSPECT commercial software.

Though the optical emission spectroscopy here performed is not spatially resolved, high-speed imaging of DEDM single discharges and 3D measurement of craters left on the workpiece surface can give some indications on possible distinct regions within the plasma. Therefore, the plasma is divided in several zones with different thickness (Δs_i) for the following calculation of the emission spectra. The total calculated emission spectra are obtained by adding up the different $\varepsilon(s)\Delta s_i$ contributions from the different plasma regions. Iterating the electron temperature, followed by a comparison with the experimental spectra, leads finally to a fit between observed and simulated emission spectra.

The dimensions of a first plasma region are based on the total plasma plume size, measured by high-speed imaging. As previously stated, the plasma plume size reaches about 400 μm for the applied experimental conditions. The craters generated from the plasma-workpiece material interactions, such as shown in Fig. 9, give also additional indications regarding different zones within the plasma. Out of this, a second plasma region is defined according to the dimensions of the craters left by single electric discharges, which have an estimated average diameter of 185 μm.

The lines intensities are simultaneously linked to the temperature and dimension of the plasma. Therefore, a proper relation between these two variables is necessary in order to obtain a synthetic spectrum that corresponds to the observed one. Although measurements of plasma plume and crater diameter provide indications about different plasma zones, it turned out that it is not possible to obtain the observed optical emission spectra using only these two dimensions. Either the experimental and simulated Al III lines are correctly fitted, whereas the simulated Al II lines get much stronger intensities than the experimental ones; or the Al II lines are properly fitted, while the intensities of the simulated Al III lines become much higher than the experimental ones.

Due to the referred reason, a third zone of the plasma is introduced to fit better the synthetic emission spectra to the observed experimental one. This third region is chosen based on the spectroscopy measurements of HAVA discharges in large gaps reported by Bacon [40] in 1975. According to his results, this region is measured to be five times smaller than the total plasma thickness. Therefore, in the present case, it is assumed a size of 80 μm for the third plasma region, localized in the centre of the discharge.

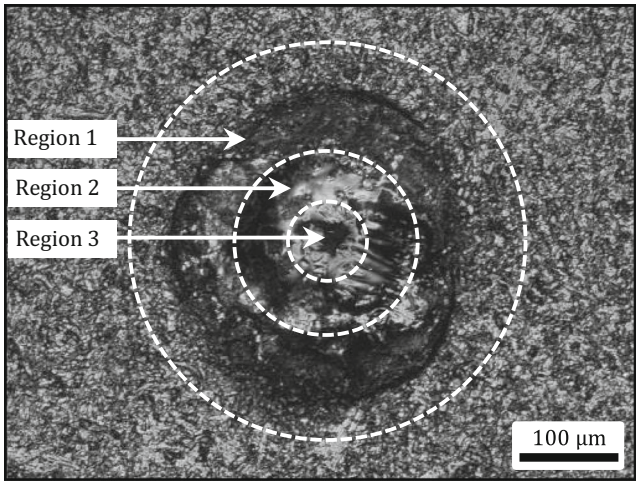

Fig. 9 Crater left by a single DEDM discharge and respective regions of the estimated plasma profile; U_{open} = 250 V; I = 20 A; t = 316 μs; Cu cathode; Al anode

Fig. 9 presents the diameters applied for the emission spectra simulation, compared with the dimensions of a crater left by a single electric discharge. The diameters are kept constant for all discharge times, although the dimensions of plasma and craters might change during the discharge development. The different components of the plasma profile are referred as regions 1, 2 and 3 in the following.

Using the presented simple three-zone model of the discharge, a good fit between calculated and experimental emission spectra is obtained for all important emission lines of all considered atomic and ionic species. It is important to state that the proposed model is a discretization of the plasma temperature profile. Further research involving spatially resolved emission spectroscopy and the application of the Abel inversion technique might provide more information about the temperature profile in the discrete or continuous form, as proposed by Sainz et al. [41].

5.3 Low-temperature plasma emission spectra simulation

A comparison of the experimental and simulated spectra of the plasma region 1 at 128 μs is shown in Fig. 10. Al I lines are emitted from excited metal vapour originating from the anode workpiece. The simulated emission spectra indicate that the plasma is mostly formed out of different Al species. It is expected from microsecond vacuum arcs with aluminium anodes under low currents, as reported in the literature [31, 40, 32].

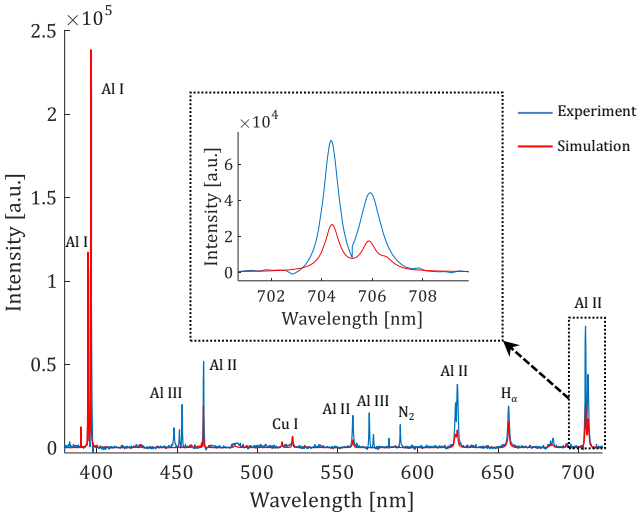

Fig. 10 Experimental and simulated emission spectra at $T = 13{,}800$ K of the plasma region 1 at 128 μs

The Cu emission lines, which emanate from the excited vapour of the cathode material, contribute only little to the spectra. For the best fitting electron temperature of intensity ratio of the Al I peaks at 394.40 and 396.15 nm, the Al II lines are weakly reproduced, as presented in the inlet of Fig. 10.

Slightly larger contribution to Al II emission lines appears by adding further the simulated emission spectra from region 2. Finally, the best fitting emission spectra, resulting from the sum of the spectra contributions from regions 1, 2 and 3, matches to most of the experimentally observed emission lines, as presented in Fig. 11.

It is important to highlight that, adding the light originating from region 3, the Al III experimental emission lines fit now to the calculated ones, as shown in the inlet of Fig. 11. The fit

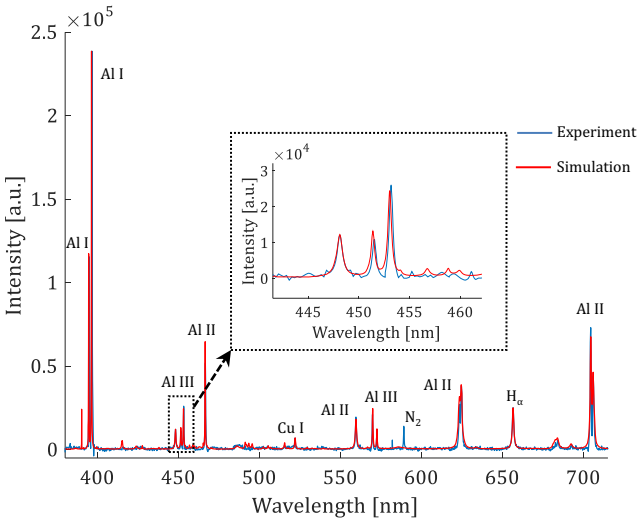

Fig. 11 Experimental and simulated emission spectra of the plasma regions 1 ($T = 13{,}800$ K), region 2 ($T = 15{,}000$ K) and region 3 ($T = 22{,}000$ K) summed at 128 μs

between experimental and simulated spectra for each time step of the electric discharge provides the time-resolved electron temperature of the different micro regions and the spatial distribution of ionic species in the plasma.

5.4 Electron temperature and burning voltage

The electron temperatures of the different plasma zones are estimated from fitting experimental and simulated emission spectra. The burning voltage provides important information about the electric discharge. The behaviour of the electron temperatures in the different plasma regions and the time-resolved RMS burning voltage are presented in Fig. 12.

The RMS burning voltage increases from around 16 to 17 V during approximately 100 μs, starting to decrease afterwards. As explained by Miller [32], this behaviour indicates a transition of the diffuse mode to an anode spot arc. The transition can be triggered by magnetic constriction of the discharge in the gap, anode melting or a combination of both phenomena. The burning voltage drop occurs between the 100 and 220 μs of the discharge due to anode material melting and the hot spot formation.

The emission spectra simulations show that the electron temperature decreases in all the regions of the plasma until the 220 μs of the discharge. It is also an indication that a hot spot is formed. The electron temperature drop probably occurs because the discharge energy is distributed over the rising metal vapour. It leads to a reduction in the average kinetic energy of the particles in the plasma. Similar results were presented by Grissom et al. [42] for microsecond vacuum arcs under low currents. Furthermore, the RMS burning voltage and the electron temperatures in the whole plasma stay relatively constant after around 220 μs. These characteristics indicate transition of a transient to a steady-state electric discharge and support the proposal made in Macedo et al. [19].

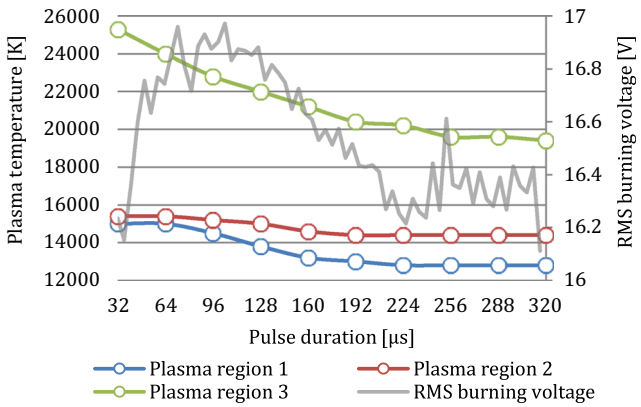

Fig. 12 Electron temperature and RMS burning voltage over time; $U_{open} = 250$ V; $I = 20$ A; Cu cathode; Al anode

5.5 Density and spatial distribution of ionic Al species

The density of particles within the plasma is associated with the erosion gap and evaporation of the anode material, which change during the discharge. The density of ions is here estimated from H_α line Stark broadening. According to the emission spectra simulations, the ion density increases almost linearly during the discharge until 160 μs, when its value becomes almost constant (Fig. 13). Similar results regarding the electron density were calculated from full width of a half maximum of the H_α line [19].

Measurements show that the electric current also increases almost linearly during the first 160 μs of the discharge and remain relatively constant later in time. It indicates a direct relation between electric discharge energy and density of ions within the plasma. Moreover, the simulations of the emission spectra are also able to provide information about the species composition in the plasma. Fig. 14 shows that the external shell of the plasma (region 1) is almost completely constituted of Al II species during the entire discharge duration.

Despite the high intensities of Al I emission lines present in the spectra, the quantity of Al I species in the plasma is proportionally very small. According to the simulations, the proportions of Al I species vary from 1 to 2% in region 1, whereas these species are not even present in region 2 (Fig. 15) and region 3 (Fig. 16). It is an indication that the whole plasma is fairly ionized.

The central and hottest zone of the plasma (region 3) is almost dominated by Al III species, whereas Al IV species are also observed at the beginning of the discharge with about 12% of the plasma composition. The Al II species increase in proportion due to the metal vapour rise, which emanates from the hot anode spot. This result is in accordance with the spectroscopic time-resolved measurements reported by Bacon [40], which shows that the most prevalent ions near the anode spot are Al III and Al IV in HAVA discharges. This characteristic also reinforces the hypothesis that anode dominated vacuum discharges are formed in DEDM.

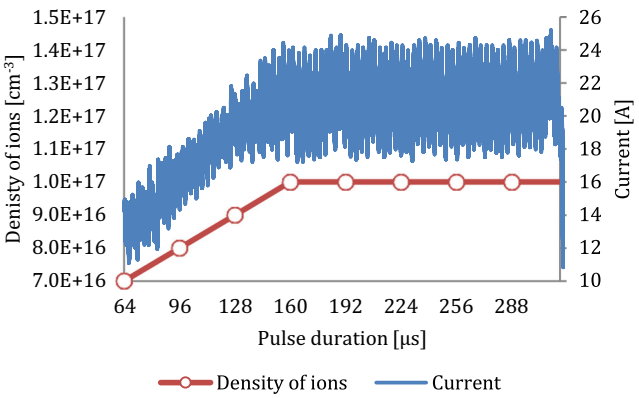

Fig. 13 Ion density of the plasma and electric current over time; U_{open} = 250 V; I = 20 A; Cu cathode; Al anode

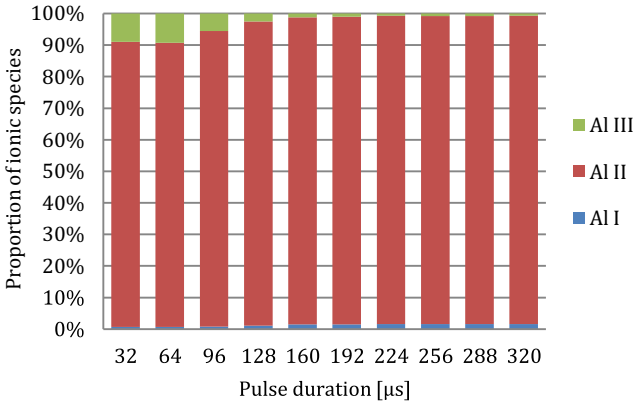

Fig. 14 Relative population of Al species in the plasma region 1; U_{open} = 250 V; I = 20 A; Cu cathode; Al anode

The estimated high temperature and large proportion of Al III species in region 3 of the plasma indicate that a hot anode spot exists with dimensions considerably smaller than the crater dimension, as schematically shown in Fig. 17.

6 Electron beam

An electron beam can also lead to the observed emission spectra, resulting in a different interpretation of the phenomena involved in the electric discharge. The presence of an electron beam can influence the dynamics of the discharge and its interactions with the electrodes. As previously mentioned, this hypothesis is also briefly presented here.

Bombardment of charged particles melts and evaporates the electrodes material, whereas ion and electron beams can be formed due to the electrical potential in front of the electrodes, anode and cathode. As proposed by Miller [43], the potential structure of the discharge can highly accelerate a fraction of the electrons, which immediately ionize the metal vapour formed near the anode. A sharp reduction of the anode potential fall (U_{Sheath}) takes place due to the ions created near

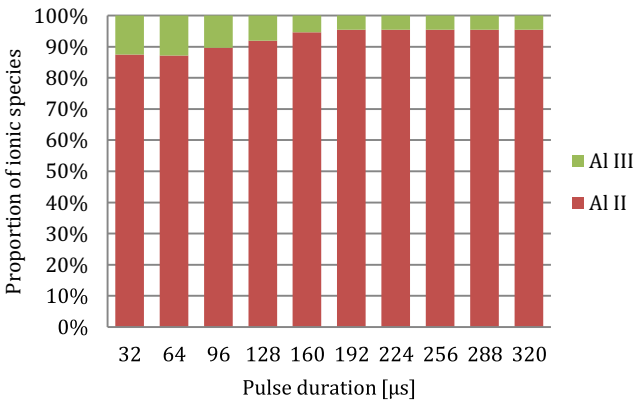

Fig. 15 Relative population of Al species in the plasma region 2; U_{open} = 250 V; I = 20 A; Cu cathode; Al anode

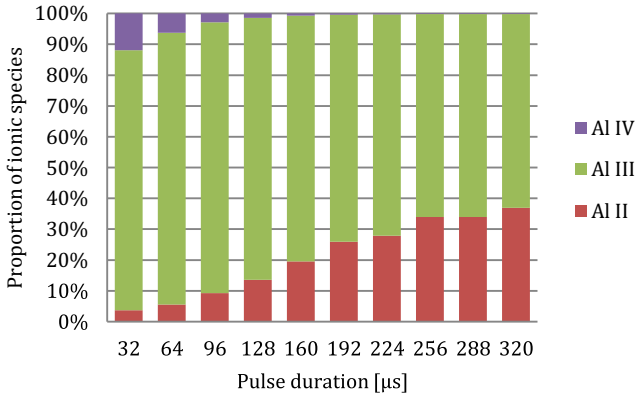

Fig. 16 Relative population of Al species in the plasma region 3; U_{open} = 250 V; I = 20 A; Cu cathode; Al anode

the electrode surface, neutralizing the space charge in the volume adjacent to the anode area, as shown in the Fig. 18.

The cathode region produces the necessary electron current to sustain the discharge, whereas part of the energy is consumed in the inter-electrode plasma column by Joule effect, heat conduction and radiation, as described by Boxman et al. [31].

The population of excited states of the different atomic and molecular species is sensitive to the high-energy component of the electron distribution in the plasma. Therefore, emission spectroscopy can also be used to diagnose non-Maxwellian electron energy distributions of plasmas in non-LTE condition. Important electron beam parameters, such as beam energy and density, can be properly estimated. Formation of an electron beam in HAVA discharges was reported by Miller [43] in large gaps in 1977. Later, the same phenomenon was suggested to take place in DEDM by Govindan et al. [4].

The resulting optical emission spectrum of an electron beam can be simulated by PrismSPECT, which allows the spectra calculation also for non-Maxwellian electron energy distributions. Fig. 19 shows a comparison between experimental spectrum from DEDM plasma and calculated emission spectrum containing an electron beam. The plasma temperatures in region 1 (size of the plasma plume) and region 2 (diameter of the formed crater) are estimated to be

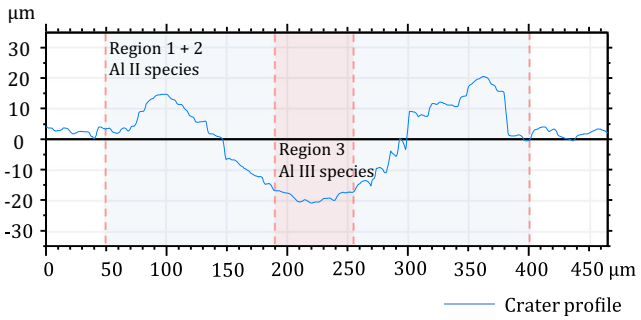

Fig. 17 Profile of a crater left by a single discharge and schematic spatial distribution of Al ionic species in the plasma

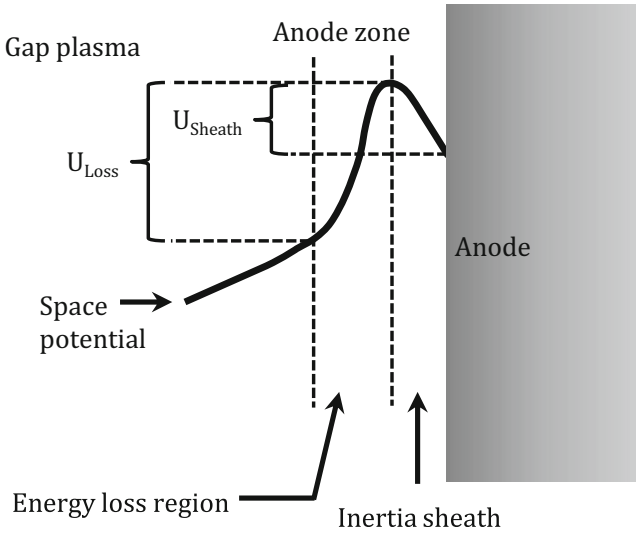

Fig. 18 Potential distribution near the anode for a high current vacuum arc at time of transition into the anode spot mode [43]

T = 13,300 K. Region 2 contains an electron beam energy E_{beam} = 8.5 eV, assuming that part of the electrical potential involves the cathode drop and the inter-electrode plasma, as proposed by Boxman et al. [31]. The used electron beam density is 6% of the total electron density of region 2.

The good fit between experimental and simulated spectra leads to the conclusion that the presence of an electron beam within the plasma can also be a possible explanation for the observed spectra. The present measurements, not spatially resolved, cannot answer to the question if an electron beam is really formed, or if only the electron temperature is peaking in the centre (region 3). Further development of spatially and time-resolved optical emission spectroscopy interpreted by emission spectra simulations is necessary in order to obtain more evidences for detailed elucidation of the electrical potential structure of the presently studied electric discharges.

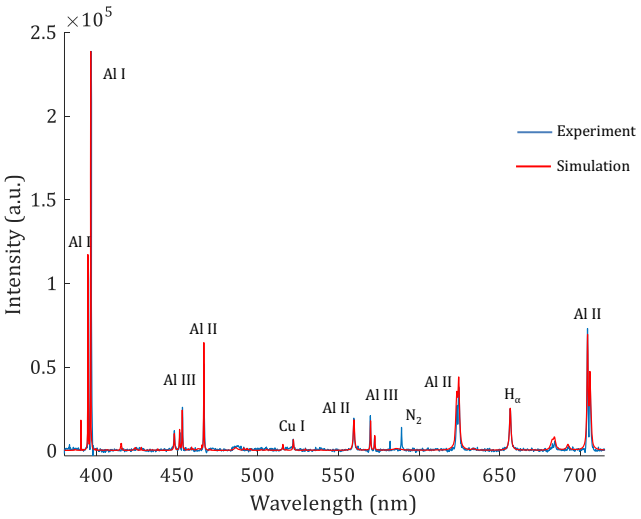

Fig. 19 Experimental and simulated emission spectra of plasma and electron beam at 128 μs; T = 13,300 K; E_{beam} = 8.5 eV

7 Conclusions

Interpretation of optical emission spectra supported by collisional-radiative models is here presented as a potential method to obtain much more information on the DEDM plasma than the ones conventionally reported in the literature. Comparisons between numerical and experimental spectra indicate that DEDM plasmas can be in LTE or non-LTE, leading to different possible interpretations of the physical phenomena involved in the electric discharges. The hypothesis of LTE is here developed, whereas the non-LTE condition is shortly introduced.

Assuming LTE condition, optical emission spectra simulations show that the estimated electron temperature profile of the plasma strongly influences the spatial distribution of ionic species. The observed ionic species are originated from ionization of the evaporated anode material, indicating that anode dominated vacuum discharges are formed.

The plasma channel is divided into three different regions for emission spectra calculations. Region 1 is the outer ring of the plasma channel. This region is characterized by a relatively low plasma temperature and is almost completely dominated by Al II species. This is an indication of a fairly ionized plasma, despite the high intensity of the observed Al I lines. Region 2 corresponds to the area of crater formation. It presents properties similar to the ones of region 1, with comparable temperatures and slightly larger contributions of Al III species to the plasma composition. Finally, the simulations show that the temperature is peaking in the centre of the plasma channel (region 3), which is almost dominated by Al III species. It indicates concentration of the discharge energy to a hot anode spot with dimension considerably smaller than the final crater diameter.

The generation of an electron beam in non-LTE plasma could also cause the same optical emission spectra as the observed experimental ones. Additional investigations, including spatially resolved emission spectroscopy, are necessary in order to explain the phenomena related to the electrical potential in the discharge.

Further interpretation than the one presented in this paper might also include an estimation of the different contaminations within plasma, originating from electrode material. Future applications of this method of optical emission spectra interpretation can be developed in combination with the well-known Abel inversion, which can give additional insight into the spatial behaviour of the micro discharges. The collisional-radiative model assisted emission spectra interpretation can also be applied to the conventional EDM in liquid dielectric media, as well as to other problems of plasma physics and plasma chemistry, where optical emission spectroscopy is an important, often the only applicable, diagnostic.

It is also important to emphasize that the characteristics of relatively inert cathode tool electrode and anode dominated discharges are very different from the ones encountered in EDM using liquid dielectric media. Thus, the search of specific electrical parameters for DEDM is necessary due to the different plasma phenomena involved in this process.

Acknowledgements We would like to thank the Swiss National Science Foundation (SNF) for funding this research.

References

1. Leão FN, Pashby IR (2004) A review on the use of environmentally-friendly dielectric fluids in electrical discharge machining. J Mater Process Technol 149(1–3):341–346. doi:10.1016/j.jmatprotec.2003.10.043
2. Kunieda M, Yoshida M, Taniguchi N (1997) Electrical discharge machining in gas. CIRP Ann Manuf Technol 46(1):143–146. doi:10.1016/S0007-8506(07)60794-X
3. ZhanBo Y, Takahashi J, Kunieda M (2004) Dry electrical discharge machining of cemented carbide. J Mater Process Technol 149(1–3): 353–357. doi:10.1016/j.jmatprotec.2003.10.044
4. Govindan P, Gupta A, Joshi SS, Malshe A, Rajurkar KP (2013) Single-spark analysis of removal phenomenon in magnetic field assisted dry EDM. J Mater Process Technol 213(7):1048–1058. doi:10.1016/j.jmatprotec.2013.01.016
5. Govindan P, Joshi SS (2010) Experimental characterization of material removal in dry electrical discharge drilling. Int J Mach Tools Manuf 50(5):431–443. doi:10.1016/j.ijmachtools.2010.02.004
6. Shen Y, Liu Y, Sun W, Zhang Y, Dong H, Zheng C, Ji R (2016) High-speed near dry electrical discharge machining. J Mater Process Technol 233:9–18. doi:10.1016/j.jmatprotec.2016.02.008
7. Kunieda M, Miyoshi Y, Takaya T, Nakajima N, ZhanBo Y, Yoshida M (2003) High speed 3D milling by dry EDM. CIRP Ann Manuf Technol 52(1):147–150. doi:10.1016/S0007-8506(07)60552-6
8. Saha SK, Choudhury SK (2009) Experimental investigation and empirical modeling of the dry electric discharge machining process. Int J Mach Tools Manuf 49(3–4):297–308. doi:10.1016/j.ijmachtools.2008.10.012
9. Roth R, Kuster F, Wegener K (2013) Influence of oxidizing gas on the stability of dry electrical discharge machining process. Procedia CIRP 6:338–343. doi:10.1016/j.procir.2013.03.029
10. Roth R, Balzer H, Kuster F, Wegener K (2012) Influence of the anode material on the breakdown behavior in dry electrical discharge machining. Procedia CIRP 1:639–644. doi:10.1016/j.procir.2012.05.013
11. Kunieda M, Takaya T, Nakano S (2004) Improvement of dry EDM characteristics using piezoelectric actuator. CIRP Ann Manuf Technol 53(1):183–186. doi:10.1016/S0007-8506(07)60674-X
12. Kunieda M, Furuoya S, Taniguchi N (1991) Improvement of EDM efficiency by supplying oxygen gas into gap. CIRP Ann Manuf Technol 40(1):215–218. doi:10.1016/S0007-8506(07)61971-4
13. Ramani V, Cassidenti ML (1985) Inert-gas electrical discharge machining. In: NASA Technical Brief NPO 15660:1985
14. Zhang QH, Du R, Zhang JH, Zhang QB (2006) An investigation of ultrasonic-assisted electrical discharge machining in gas. Int J Mach Tools Manuf 46(12–13):1582–1588. doi:10.1016/j.ijmachtools.2005.09.023
15. Joshi S, Govindan P, Malshe A, Rajurkar K (2011) Experimental characterization of dry EDM performed in a pulsating magnetic field. CIRP Ann Manuf Technol 60(1):239–242. doi:10.1016/j.cirp.2011.03.114

16. Shen Y, Liu Y, Zhang Y, Dong H, Sun W, Wang X, Zheng C, Ji R (2015) High-speed dry electrical discharge machining. Int J Mach Tools Manuf 93:19–25. doi:10.1016/j.ijmachtools.2015.03.004
17. Tao J (2008) Investigation of dry and near-dry electrical discharge milling process. University Of Michigan
18. Kanmani Subbu S, Karthikeyan G, Ramkumar J, Dhamodaran S (2011) Plasma characterization of dry μ-EDM. Int J Adv Manuf Technol 56(1–4):187–195. doi:10.1007/s00170-011-3162-4
19. Macedo FTB, Wiessner M, Hollenstein C, Kuster F, Wegener K (2016) Investigation of the fundamentals of tool electrode wear in dry EDM. Procedia CIRP 46:55–58. doi:10.1016/j.procir.2016.03.170
20. MacFarlane JJ, Golovkin IE, Wang P, Woodruff PR, Pereyra NA (2007) SPECT3D—a multi-dimensional collisional-radiative code for generating diagnostic signatures based on hydrodynamics and PIC simulation output. High Energy Density Physics 3(1–2):181–190. doi:10.1016/j.hedp.2007.02.016
21. Descoeudres A (2006) Characterization of electrical discharge machining plasmas. EPFL
22. Maradia U (2014) Meso-micro EDM. Zürich, ETH-Zürich
23. Loeb LB, Meek JM (1941) The mechanism of the electric spark. Stanford University Press
24. Raizer YP (1991) Gas discharge physics. Springer-Verlag, Berlin; New York
25. Meek JM, Craggs JD (1978) Electrical breakdown of gases. Wiley
26. Toyota H, Zama S, Akamine Y, Matsuoka S, Hidaka K (2002) Gaseous electrical discharge characteristics in air and nitrogen at cryogenic temperature. Dielectrics and Electrical Insulation, IEEE Transactions on 9(6):891–898. doi:10.1109/TDEI.2002.1115482
27. Torres JM, Dhariwal RS (1999) Electric field breakdown at micrometre separations. Nanotechnology 10(1):102
28. Ching-Heng C, Yeh JA, Pei-Jen W (2006) Electrical breakdown phenomena for devices with micron separations. J Micromech Microeng 16(7):1366
29. Dhariwal RS, Torres JM, Desmulliez MPY (2000) Electric field breakdown at micrometre separations in air and nitrogen at atmospheric pressure. Science, Measurement and Technology, IEE Proceedings 147(5):261–265. doi:10.1040/ip-smt:20000506
30. Klas M, Matejćik Š, Radjenović B, Radmilović-Radjenović M (2011) Experimental and theoretical studies of the breakdown voltage characteristics at micrometre separations in air. EPL (Europhysics Letters) 95(3):35002
31. Boxman RL, Sanders DM, Martin PJ (1995) Handbook of vacuum arc science and technology: fundamentals and applications. Noyes Publications
32. Miller HC (1983) Vacuum-arc anode phenomena. IEEE Transactions on Plasma Science 11(2):76–89. doi:10.1109/tps.1983.4316225
33. Jakubowski L, Sadowski MJ (2002) Hot-spots in plasma-focus discharges as intense sources of different radiation pulses. Braz J Phys 32:187–192
34. Bacon FM, Watts HA (1975) Vacuum arc anode plasma 2. Collisional-radiative model and comparison with experiment. J Appl Phys 46(11):4758–4766. doi:10.1063/1.321553
35. Macedo FTB, Wiessner M, Hollenstein C, Kuster F, Wegener K (2016) Dependence of crater formation in dry EDM on electrical breakdown mechanism. Procedia CIRP 42:161–166. doi:10.1016/j.procir.2016.02.212
36. Kojima A, Natsu W, Kunieda M (2008) Spectroscopic measurement of arc plasma diameter in EDM. CIRP Ann Manuf Technol 57(1):203–207. doi:10.1016/j.cirp.2008.03.097
37. Kunze HJ (2009) Introduction to plasma spectroscopy. Springer, Berlin Heidelberg
38. Gigosos MA, Cardeñoso V (1996) New plasma diagnosis tables of hydrogen stark broadening including ion dynamics. J Phys B Atomic Mol Phys 29(20):4795
39. Griem HR (1997) Principles of plasma spectroscopy. Cambridge University Press
40. Bacon FM (1975) Vacuum arc anode plasma. I. Spectroscopic investigation. J Appl Phys 46(11):4750–4757. doi:10.1063/1.321552
41. Sainz A, Diaz A, Casas D, Pineda M, Cubillo F, Calzada MD (2006) Abel inversion applied to a small set of emission data from a microwave plasma. Appl Spectrosc 60(3):229–236. doi:10.1366/000370206776342706
42. Grissom JT, Newton JC (1974) Anode surface radiance from microsecond vacuum arcs. J Appl Phys 45(7):2885–2894. doi:10.1063/1.1663696
43. Miller HC (1977) Vacuum arc anode phenomena. IEEE Transactions on Plasma Science 5(3):181–196. doi:10.1109/TPS.1977.4317037